Indian Journal of Chemistry
Vol. 60A, June 2021, pp. 812-823

Transition metal ion (Ni^{2+}, Cu^{2+} and Zn^{2+}) doped defect pyrochlore, $KTaTeO_6$: Synthesis, characterization and photocatalytic studies

M Sudheera[a], P Venkataswamy[b], K Ramaswamy[b,c], G Ravi[b], N Chittibabu[d] & M Vithal[b,*]

[a]Department of Chemical Engineering, RVR and JC College of Engineering, Chowdavaram, Guntur 522 019, India

[b]Department of Chemistry, University College of Science, Osmania University, Hyderabad 500 007, India

[c]Centre for Materials for Electronics Technology (C-MET), Cherlapally, HCL (PO), Hyderabad 500 051, India

[d]Department of Chemical Engineering, Andhra University, Visakhapatnam 530 003, India

*E-mail: mugavithal@gmail.com

Received 08 February 2021, revised and accepted 31 March 2021

One of the strategies to decrease the bandgap energy and increase the optical absorption of the catalysts is to dope with transition metal ions. In this paper, the results obtained for the degradation of methylene blue (MB) pollutant in the presence of M^{2+} (M = Ni, Cu, and Zn) doped $KTaTeO_6$ (M-KTTO) upon visible light irradiation are presented. The parent $KTaTeO_6$ and the M-$KTaTeO_6$ were prepared by solid-state and ion-exchange methods, respectively. All the samples were characterized by XRD, SEM/EDX, FT-IR, UV-vis DRS, XPS, and PL techniques. The metal ion doping in place of K^+ has influenced the electronic and optical properties considerably. The doping of M^{2+} into KTTO lattice has narrowed the bandgap energy, increased the visible light absorbance leading to higher photocatalytic activity. The M-KTTO materials show higher photocatalytic activity compared to parent KTTO, particularly Cu-KTTO. The scavenging experiments indicate that $^{\bullet}OH$ radicals are the main active species involved in the photodegradation of MB. The Cu-KTTO is chemically stable and can be used for at least up to five cycles. The mechanistic pathway of MB degradation was proposed over Cu-KTTO.

Keywords: $KTaTeO_6$, Transition metal ions, Ion-exchange method, Bandgap energy, MB degradation, $^{\bullet}OH$ radicals

Wastewater effluent from various industries and households often containing tenacious organic (major) and inorganic (minor) pollutants and contaminate the water bodies[1,2]. These chemicals have to be removed to improve the quality of water before being used in the agriculture and domestic sectors. Wastewater treatment is also essential to minimize the damage to the ecological system[3]. Although the traditional methods such as adsorption, coagulation, ultra-filtration, and advanced oxidation process (AOP), etc., are in practice, they are either expensive or release secondary pollutants[4]. AOP methods are found to be suitable in the degradation of organic pollutants. Semiconductor-mediated photocatalysis, one of the AOPs, is cost-effective and requires minimum instrumentation[5,6]. If the bandgap energy of the semiconductor falls in the visible range (< 3 eV), abundant sunlight can be employed to reduce the cost further. Thus, designing a visible light active photocatalyst is a challenge to both the scientific and industrial community.

Pyrochlore is one of the two common oxide textbook structures with potential applications in various fields, the other being perovskite. An ideal pyrochlore structure crystallizes in a cubic lattice with the general formula $A_2B_2O_6O'$. These oxides can be synthesized under different experimental conditions when cations (A and B) have suitable valency and size. The common charge combinations are (A^{3+}, B^{4+}) and (A^{2+}, B^{5+}) with the radius ratio limit $1.93 < (r_A/r_B) < 2.75$, although the extreme limits are scanty. The structure of ideal pyrochlore is characterized by corner-sharing of BO_6 octahedral units and A_2O' chains. The A and B ions possess six and eight coordination respectively[7]. The zig-zag A_2O' chains are interpenetrating into the octahedral units leading to a three-dimensional framework structure with tunnels. The interactions between BO_6 units and A_2O' chains are very weak and the structure and stability are retained even when vacancies at A site or O' site or both sites, are created. The resultant compositions $A_2B_2O_6$ (O' vacancy) and AB_2O_6 (A and O' vacancies), called "defect pyrochlore", also crystallize in a cubic lattice. Often, these defect pyrochlores are hydrated. The water molecules reside in the tunnels. These defect pyrochlore oxides have remarkable ion-exchange properties.

Defect pyrochlores containing niobium and tantalum exhibit good ionic conductivity and ion-exchange properties. They find applications in solid electrolyte fuel cells and conversion of hydrocarbons[8]. The ion exchange property of a few Sb, Ti, Ta, Nb, W containing defect pyrochlore compositions was exploited to remove radioactive ions[9,10]. Britvin *et al*. have investigated the ion exchange properties of two niobium containing defect pyrochlores ($NH_4Nb_2O_5(OH, F)$ and $KNb_2O_5(OH, F).nH_2O$)[11]. Cations such as Sr^{2+}, Ba^{2+}, Cd^{2+}, Pb^{2+}, Co^{2+}, Ni^{2+}, and Cu^{2+}, were selectively exchanged by this two niobium containing defect pyrochlores[11]. Additionally, some oxides with defect pyrochlore structure with general formula AB_2O_6 have been investigated as photocatalysts for dye degradation[7,12]. For example, Waehayee *et al*. synthesized the $KNbTeO_6$ and ion-exchanged with Ag^+, Cu^{2+}, and Sn^{2+} for photodegradation of methylene blue (MB) under visible light irradiation[13]. In our previous work, synthesis of $KTaTeO_6$ and Ag-doped $KTaTeO_6$ was reported and photocatalytic activity for degradation of methyl violet and hydrogen evolution was studied[14]. In continuation of our search for better photocatalytic materials, we have chosen defect pyrochlore, $KTaTeO_6$, and doping it with transition metal ions (Ni^{+2}, Cu^{2+}, and Zn^{2+}) into its lattice to enhance the visible light photoactivity against the degradation of dyes. It is known that the incorporation of transition metal ions into metal oxides can create new energy levels within a bandgap which primarily improves the charge separation efficiency of e^--h^+ by forming electron traps, thus enhancing the photocatalytic activity[15,16]. To our knowledge, the doping of transition metal ions into tellurium-containing defect pyrochlores for photocatalytic dye degradation is not studied.

Against the above background, an attempt is made to prepare parent $KTaTeO_6$ and M^{2+}-doped $KTaTeO_6$ (M = Ni, Cu, and Zn) by solid-state and ion exchange methods, respectively. The goal of the current study is to evaluate the effect of transition metal ion doping on the photocatalytic activity of $KTaTeO_6$ against MB degradation and the corresponding results were compared.

Materials and Methods

Preparation of $KTaTeO_6$ (KTTO)

Parent KTTO was prepared by the solid-state method. In brief, K_2CO_3 (SDFCL, 99.99%), Ta_2O_5, and TeO_2 (Sigma Aldrich, 99.99%) were weighed and intimately crushed in an agate mortar in the presence of acetone[14]. The K:Ta:Te molar ratio was 0.5:0.5:1. The well-ground mixture was heated in powder form in an alumina crucible with three thermal treatments, at 300 ºC for 5 h, 400 ºC for 10 h, and at 600 ºC for 16 h. After each heat treatment, the sample was thoroughly grounded to attain better homogeneity. At the end of the final heat treatment, a brick red colored sample was obtained.

Preparation of Ni^{2+}, Cu^{2+} and Zn^{2+} doped $KTaTeO_6$

The ion-exchange method was used to prepare Ni, Cu, and Zn-doped KTTO. For the preparation of Ni and Cu-doped KTTO, the $NiCl_2.6H_2O$ (98%, SDFCL), and $CuCl_2.2H_2O$ (98%, SDFCL) were used, respectively. To prepare Ni-KTTO, 0.5 g of parent KTTO (0.001 mol) was stirred with 100 mL of 0.02 M $NiCl_2.6H_2O$ (0.002 mol) solution for 24 h at room temperature (27 ºC) to ensure maximum ion exchange. The resultant solid was washed several times with double distilled water and dried at 100 ºC in air. A similar procedure was adopted to prepare the Cu-doped KTTO catalyst with a 0.02 M solution of $CuCl_2.2H_2O$ (0.002 mol). To prepare Zn-doped $KTaTeO_6$, a stoichiometric amount of ZnO (0.002 mol) was dissolved in dilute HCl and heated at 100 ºC to remove the excess HCl. The resultant material was dissolved in 100 mL double distilled water. The as-obtained $ZnCl_2$ was mixed with 0.5 g of parent KTTO (0.001 mol) at room temperature and stirred for 24 h to confirm maximum ion exchange. The solid obtained was washed several times with double distilled water and dried at 100 ºC in air. The Ni, Cu, and Zn-doped $KTaTeO_6$ catalysts are referred to as Ni-KTTO, Cu-KTTO, and Zn-KTTO, respectively.

Characterization techniques

Powder X-ray diffraction (XRD) patterns were obtained using a Rigaku miniplex diffractometer (40 kV, 15 mA) using Cu-Kα1 radiation (λ = 1.5406 Å). The data were recorded between 10º and 80º (2θ) in steps of 0.01 º/min with a count time of 1s per step. The surface morphologies of the samples were recorded on a JEOL JSM-6610 scanning electron microscope equipped with an EDX Inc. energy-dispersive X-ray detector for elemental analysis. The FT-IR spectra were recorded in the range of 250–4000 cm^{-1} with 2 cm^{-1} resolution using a Jasco IR-5300 spectrometer in the form of thin KBr pellets. The ultraviolet-visible (UV–vis) diffuse reflectance

spectra were measured by a Jasco V650 UV-vis spectrophotometer in the range of 200-800 nm using $BaSO_4$ as the reference standard. X-ray photoelectron spectroscopy (XPS) studies were performed with the help of a K-α spectrometer (Thermo Scientific) having a source of Al-Kα radiation (hυ= 1486.7 eV) at room temperature under ultra-high vacuum (10^{-8} Pa). Photoluminescence (PL) spectra were recorded using a JASCO FP-8500 spectrofluorometer with an excitation wavelength of 250 nm at room temperature.

Photocatalytic experiments

The photocatalytic efficiency of synthesized samples was studied by the degradation of MB under visible light irradiation using HEBER visible annular type photoreactor. A 300 W tungsten lamp (380 nm < λ < 840 nm) was used as the visible light source. 50 mg photocatalyst was dispersed in 50 mL of aqueous MB solution (initial concentration = 1×10^{-5} M) and kept under stirring for 60 min in the dark to attain adsorption-desorption equilibrium. The samples were taken out after an equal interval of time (30 min), filtered and examined via ultraviolet-visible spectrometer (on a JASCO V650) to evaluate the degraded amount of MB dye.

Mechanistic studies of photocatalyst

To investigate the reactive species directly involved in the photodegradation over the Cu-KTTO, the radical trapping experiments were performed. For this purpose, 2 mM concentration of different scavengers such as isopropyl alcohol (IPA), benzoquinone (BQ) and ammonium oxalate (AO) were used to trap the generated $^{\bullet}OH$, $^{\bullet}O_2^-$, and h^+ species, respectively, during the degradation process[17]. The method was similar to the above photocatalytic activity test. In addition, the generation of $^{\bullet}OH$ formed during photocatalytic degradation in the presence of Cu-KTTO was detected by the PL technique with an excitation wavelength of 250 nm, using terephthalic acid (TA) as probe molecule[18].

Results and Discussion

The crystalline structure and phase purity of parent, Ni, Cu and Zn doped KTTO were examined using XRD analysis and the obtained patterns of all these samples are shown in Fig. 1. It is seen that all the diffraction peaks can be indexed to the cubic structure of $KTaTeO_6$ (JCPDS No. 25-0683, space group *Fd3m*)[14]. The XRD peaks observed at 2θ = 15.1, 28.9, 30.3, 35.1, 38.3, 46.1, 50.3, 52.7, 59.1, 59.8, 62.7, 64.9, 70.6 and 73.8 for parent KTTO, correspond to (111), (311), (222), (400), (331), (511), (440), (531), (533), (622), (444), (551), (731), and (800) crystal planes, respectively (JCPDS card No. 25-0683)[14]. The XRD patterns of Ni-KTTO, Cu-KTTO and Zn-KTTO samples are akin to each other and comparable with pristine KTTO pattern as shown in Fig. 1a. Thus the crystal lattice of KTTO is unchanged upon doping with divalent Ni, Cu and Zn ions. No impurity peaks were observed in the diffraction patterns of Ni-KTTO, Cu-KTTO and Zn-KTTO suggesting the incorporation of Ni^{2+}, Cu^{2+} and Zn^{2+} into KTTO lattice. Further, the presence of narrow linewidth and intense diffraction peaks in the XRD patterns indicate that parent and doped KTTO samples are highly crystalline. Another notable feature of these patterns is that the diffraction lines of Ni-KTTO, Cu-KTTO, and Zn-KTTO catalysts are

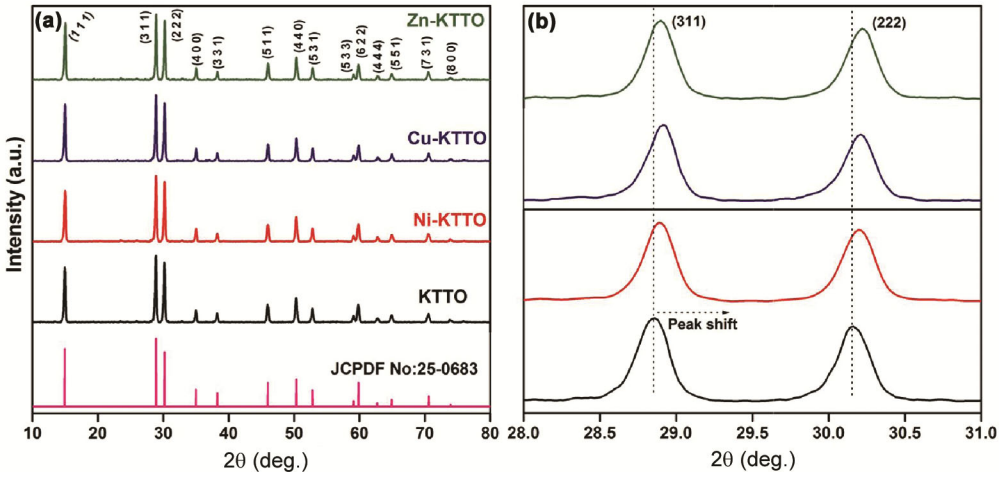

Fig. 1 — (a) Powder XRD patterns of KTTO, Ni-KTTO, Cu-KTTO and Zn-KTTO and (b) represents the peak shift of d-lines in the 2θ (28º –30º) region

slightly shifted to higher 2θ concerning KTTO (Fig. 1b). The observation of shifting of diffraction peaks to a higher 2θ value indicates that transition metal ions are successfully doped into the KTTO lattice. The least-square fitting of observed *d*-lines (using POWD software) shows a decrease in unit cell parameter as shown in Table 1. This is in accordance with the ionic sizes of doped transition metal ions (0.72 Å for Ni^{2+}, 0.73 Å for Cu^{2+}, 0.74 Å for Zn^{2+}) substituting for K^+ (1.51 Å) in the pyrochlore lattice[19,20]. Moreover, doping of transition metals into KTTO causes line broadening which is leading to inhibition in crystal growth. The crystallite size of each sample, calculated using Scherrer's equation for (311) diffraction peak and the values are 36.7, 34.8, 33.4 and 34.2 nm for KTTO, Ni-KTTO, Cu-KTTO and Zn-KTTO, respectively (Table 1). The structure of cubic $KTaTeO_6$ consists of a three-dimensional framework of $[TaO_6]$ and $[TeO_6]$ octahedra sharing vertices, forming large cages wherein potassium ions are distributed in order to maintain the charge balance as shown in Fig. 2[21].

The morphology of all the samples was studied by SEM analysis. In Supplementary Data, Fig. S1 shows the SEM images of as-prepared samples. As shown in Fig. S1a, it is clear that parent KTTO possesses randomly distributed hexagonal-shaped crystallites of different sizes. The morphology of transition metal ion-doped KTTO compositions is distinct from that of parent KTTO. The SEM images of Ni-KTTO, Cu-KTTO and Zn-KTTO show uneven distribution of quasi-spherical shaped particles with considerable agglomeration. EDX analysis is also performed to investigate the elemental composition of synthesized materials (Supplementary Data, Fig. S2). The EDX spectra of parent KTTO reveal the presence of K, Ta, Te and O elements. The EDX spectra of transition metal ion-doped KTTO compositions contain Ta, Te, O peaks in all compositions and Ni, Cu, and Zn peaks in Ni-KTTO, Cu-KTTO, and Zn-KTTO samples, respectively. This result confirms that the Ni^{2+}, Cu^{2+} and Zn^{2+} ions are successfully doped into the $KTaTeO_6$ lattice. Further, no impurity peak is observed in the detection limit of EDX demonstrating the high purity of prepared samples. The atomic percentages of elements present in as-synthesized samples are given in Supplementary Data, Table S1.

FT-IR spectra were recorded in the 4000–250 cm^{-1} range to identify the presence of O-H and Ta/Te-O bonding modes in all the synthesized catalysts and shown in Fig. 3. It is noticed that the FT-IR spectra of Ni-KTTO, Cu-KTTO and Zn-KTTO are similar to each other and consistent with that of the parent KTTO IR spectrum. However, Ni-KTTO, Cu-KTTO and Zn-KTTO compositions show additional bands at 3450, 1630 and 1120 cm^{-1}. The broad absorption band

Table 1 — The crystallite size (D) , lattice parameter (LP) and lattice volume (LV) of KTTO, Ni-KTTO, Cu-KTTO and Zn-KTTO

Sample	D (nm)	LP (Å)	LV ($Å^3$)
KTTO	36.7	10.25	1076.89
Ni-KTTO	34.8	10.251	1077.21
Cu-KTTO	33.4	10.255	1078.46
Zn-KTTO	34.2	10.253	1077.84

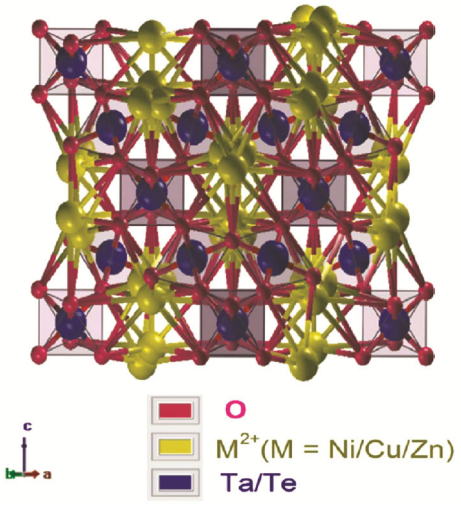

Fig. 2 — Schematic crystal structure of transition metal doped-$KTaTeO_6$

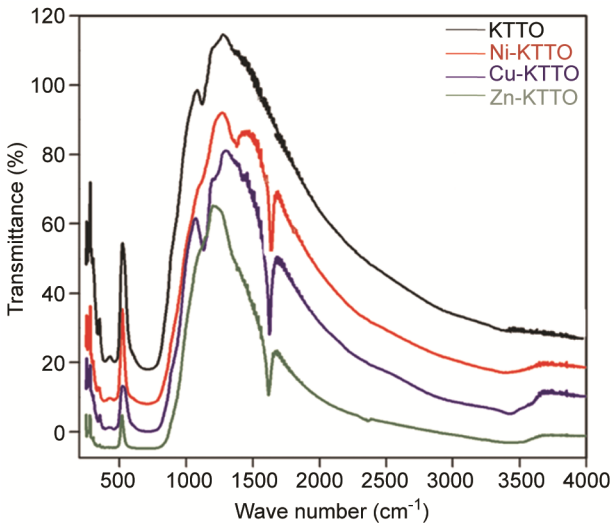

Fig. 3 — FT-IR spectra of KTTO, Ni-KTTO, Cu-KTTO and Zn-KTTO

at 3450 cm^{-1} is related to O–H stretching vibrations, whereas the band near 1630 cm^{-1} represents H–O–H bending vibration of surface/lattice water. The less intense band at ~1,085 cm^{-1} is due to M–OH bending vibrations of catalysts[22]. As the Ni-KTTO, Cu-KTTO and Zn-KTTO samples are prepared in the aqueous medium, a small quantity of water might have been adsorbed on the catalysts or entered into its cubic lattice. The absence of these bands in the infrared spectrum of KTTO confirms that it is free from adsorbed or lattice water. Two strong bands in the region 520–700 and 380–470 cm^{-1} are assigned to (Ta/Te)-O stretching and bending vibration modes in $(Te/Te)O_6$ octahedra, respectively[13,23]. Furthermore, these bands are usually broadened in the doped samples probably due to distortions in the Ta/Te–O octahedra as a result of the replacement of potassium ions by transition metal ions. The two weak bands observed at 270 and 330 cm^{-1} are due to the bending modes of Ta/Te–O[24].

The UV–vis DRS measurements were recorded to evaluate the influence of transition metal doping on the optical properties KTTO (Fig. 4 (a-d)). All the samples have shown three absorption peaks in the UV-region with peak maxima at 255, 290 and 380 nm. These peaks can be due to the oxygen-to-metal charge transfer transitions, corresponding to the electronic excitation from the valence band to the conduction band[19]. The pristine KTTO sample exhibits an absorption edge at 565 nm while the Ni-KTTO, Cu-KTTO, Zn-KTTO compositions have shown a significant redshift (shift towards longer wavelength) concerning the parent KTTO, which indicates that bandgap was narrowed after doping of transition metal ions. This result implies that the electronic structure of $KTaTeO_6$ was altered by the doping of transition metal ions. This is possibly due to the introduction of impurity energy levels below the conduction band and within the bandgap states of KTTO[16]. The absorption shift towards the higher wavelength of the prepared samples is found to follow the order: Cu-KTTO > Zn-KTTO > Ni-KTTO > KTTO. The absorption profiles were converted to Kubelka-Munk functions to estimate the bandgap energies of doped samples. The calculated bandgap values are found to be 2.47, 2.14, 2.11, and 1.95 eV for KTTO, Ni-KTTO, Zn-KTTO, and Cu-KTTO samples, respectively (insets in Fig. 4)[2]. The obtained results indicated that the bandgap of KTTO was decreased considerably after doping with transition

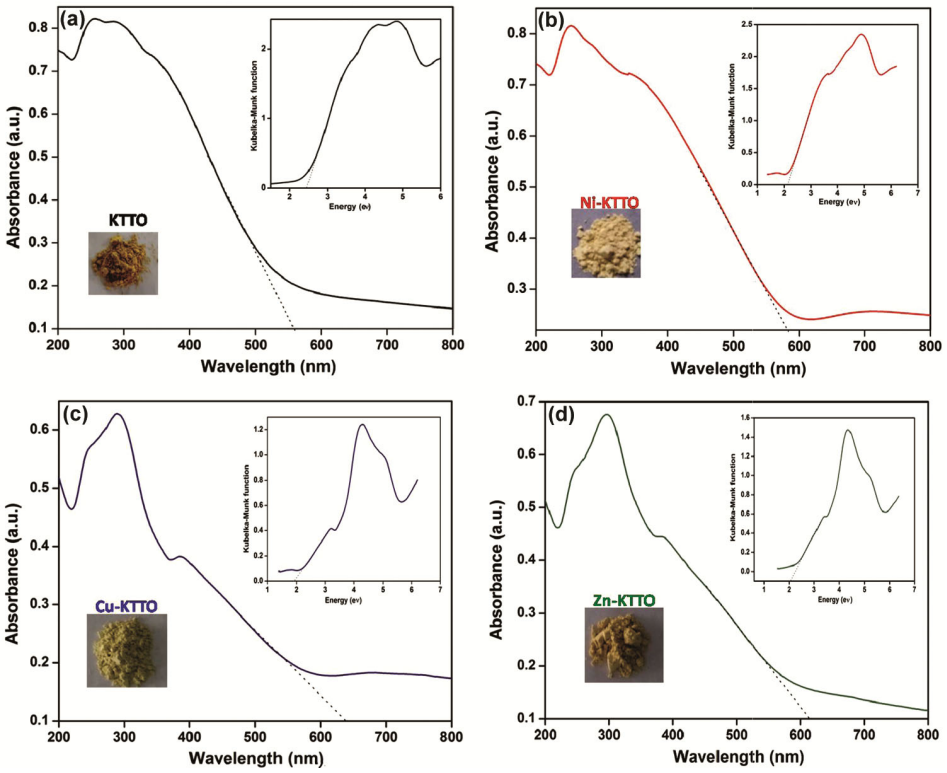

Fig. 4 — UV-vis DRS spectra of (a) KTTO, (b) Ni-KTTO, (c) Cu-KTTO and (d) Zn-KTTO (The insets present the corresponding plots of KM-function versus energy (hν) and colors of the respective samples)

metal ions. Another notable feature of transition metal ion doping is the change in color of the samples. The parent KTTO shows a brick-red color, while, all the transition metal doped KTTO materials show yellow to light yellow color, suggesting their ability to absorb light in the visible region (insets in Fig. 4). A decrease in bandgap energy may favour higher absorption of photons and hence a higher photocatalytic activity towards dye degradation.

The surface composition and oxidation states of elements present in KTTO and Cu-KTTO (representative of doped compositions) samples were examined by XPS measurements. The representative spectra were calibrated with C1s as standard at 284.6 eV. The XPS spectra of elements were analyzed based on reported results. The XPS survey spectra of KTTO and Cu-KTTO are shown in Fig. 5a. As shown in Fig. 5a, the parent KTTO is composed of K, Ta, Te and O elements, while that of Cu-KTTO contains Cu,

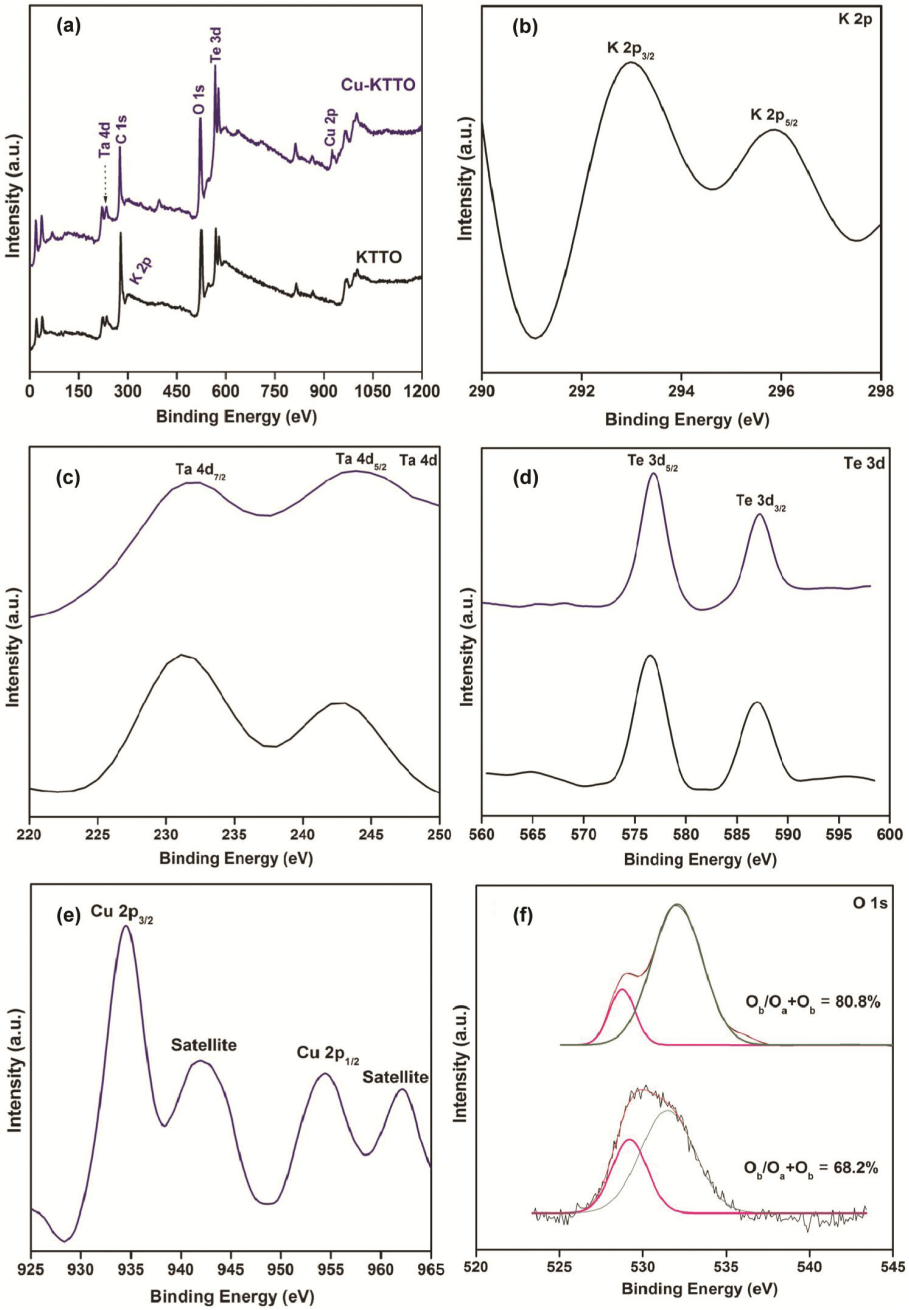

Fig. 5 — XPS spectra of KTTO and Cu-KTTO: (a) survey scan spectrum, (b) K 2p, (c) Ta 4d, (d) Te 3d, (e) Cu 2p, and (f) O 1s

Ta, Te, and O elements. These results are consistent with the EDX findings. The XPS results also indicate that both compositions are free from impurities. In Fig. 5b, two peaks located at 292.9 and 295.7 eV are characteristic of K^+ species and were assigned to $2p_{3/2}$ and $2p_{1/2}$ states, respectively of this ion[25]. The Ta 4d spectrum (Fig. 5c) exhibited two peaks at about 231.2-231.6 and 242.8-243.2 eV, corresponding to $4d_{7/2}$ and $4d_{5/2}$ states, respectively, confirming the existence of Ta^{5+}. These values are in accordance with reported values[26]. The binding energy values observed at 576.5-576.8 and 587.1-587.4 eV (Fig. 5d) can be assigned to Te $3d_{5/2}$ and Te $3d_{3/2}$ states, respectively, in its +6 oxidation state in both KTTO and Cu-KTTO samples. The difference in energy of $3d_{5/2}$ and $3d_{3/2}$ states is 10.6 eV corresponding to the spin-orbit coupling of Te^{+6} species[17]. Fig. 5e depicts the Cu 2p XPS spectrum of the Cu-KTTO sample. The distinct peaks located at 934.4 eV and 954.4 correspond to Cu $2p_{3/2}$ and $2p_{1/2}$ states, respectively, indicating the presence of Cu^{2+} in Cu-KTTO. The difference in energy of Cu $2P_{3/2}$ and $2P_{1/2}$ is 20 eV and corresponds to the spin-orbit coupling of Cu^{2+} and validates the presence of copper in +2 oxidation state[27]. The presence of satellite peaks at 942.1 and 962.1 eV also confirmed the Cu^{2+} state in Cu-KTTO. The broad peak observed in the 529-532 eV range corresponds to O 1s binding energy (Fig. 5f). This peak is deconvoluted into two peaks centered at 529.2 and 531.5 eV. The peak at 529.2 eV can be attributed to the lattice oxygen (O^{2-} from the crystal lattice and designed as O_a), while the peak at higher binding energy (531.5 eV) corresponds to the surface adsorbed oxygen species (denoted as O_b) such as -OH, O_{ads}, and OH^-, respectively[28].

It is believed that the surface adsorbed oxygen species strongly influence photocatalytic activity. They act as trapping centers for photoinduced holes which leads to the generation of a higher amount of hydroxyl radicals and hence higher photocatalytic activity[29]. The relative concentration of O_b ($O_b = O_b/O_a+O_b$) is obtained from its area under the peak. The concentration of O_b is found to be 68.2% and 80.8% for KTTO and Cu-KTTO, respectively. Thus Cu-KTTO is expected to exhibit higher photocatalytic activity compared to that of parent KTTO. It is noteworthy that the binding energies of Ta 4d, Te 3d and O 1s are slightly shifted to higher values in Cu-KTTO in comparison with KTTO. This may be due to the change in the chemical environment of oxygen ions (K-O-Ta/Te) that resulting from the doping of K^+ by Cu^{2+} ions in the crystal lattice.

It is well documented that the charge separation efficiency of the photogenerated electron-hole pairs is a key point in the process of photocatalytic reaction[3]. The PL spectroscopic study is an important and effective technique to examine such phenomena in semiconducting materials. Lower the PL intensity, the charge separation will be higher and expected to exhibit higher photocatalytic activity. Given this, the PL emission spectra of the as-synthesized materials were measured at an excitation wavelength of 250 nm and the results are shown in Fig. 6. It is seen that all the transition metal doped KTTO samples show lower PL emission intensity than that of the pure KTTO, due to the introduction of impurity energy level formed below the conduction band and within the bandgap states of KTTO. The introduction of such energy levels is known to act as charge traps for photoinduced electrons, which reduced the recombination of charge carriers. In the present investigation, the intensity of the PL emission decreases in the order: KTTO > Ni-KTTO > Zn-KTTO > Cu-KTTO. Thus the composition Cu-KTTO has the lowest PL emission intensity suggesting that the Cu^{2+} doping leads to better separation efficiency and hence expected to exhibit better photocatalytic activity.

Photocatalytic activity

The photocatalytic activity of all the synthesized metal ion-doped catalysts was investigated in aqueous medium under visible light irradiation at room temperature against the degradation of MB.

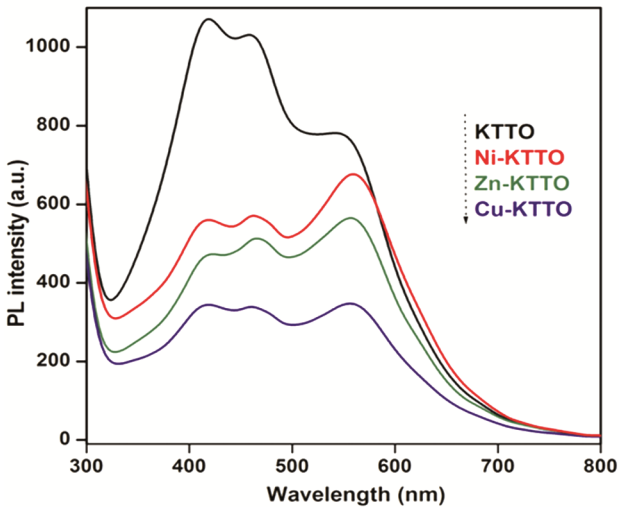

Fig. 6 — PL spectra of KTTO, Ni-KTTO, Cu-KTTO and Zn-KTTO

The UV-vis absorption spectra MB in the presence of parent KTTO, Ni-KTTO, Cu-KTTO, and Zn-KTTO for the different irradiation times (0 to 180 min) are shown in Figs. 7 (a-d), respectively. It is observed that the intensity of the characteristic absorbance of MB at a wavelength of 663 nm decreased with the increase in irradiation time, and this decrease in intensity shows a different trend with each photocatalyst[18]. Fig. 8a shows the photocatalytic degradation behavior of the MB with irradiation time in the presence of different catalysts along with the blank test. As shown in figure 8a, a blank experiment (without catalyst) shows about 11% degradation of MB after 180 min of visible light irradiation. This corresponds to the photolysis of MB dye. The degradation of MB in the presence of KTTO, Ni-KTTO, Cu-KTTO, and Zn-KTTO catalysts after 180 min of visible light irradiation is 82%, 89%, 96% and 92% respectively. Compared to pristine KTTO, all the transition metal ion-doped KTTO have shown higher photocatalytic activity which may be due to the lower recombination rate of e^--h^+ pairs in doped compositions. It was found that the photocatalytic efficiency of the synthesized catalysts was varying in the order of Cu-KTTO > Zn-KTTO > Ni-KTTO > KTTO. The remarkable photocatalytic activity of Cu-KTTO can be principally assigned to its lower bandgap energy with more separation efficiency of photoinduced electron-hole pairs. The kinetics of MB degradation with all the synthesized catalysts was also studied and the corresponding data presented in Fig. 8b. As shown in this figure, a good linear relationship between $\ln(C_0/C)$ against irradiation time was found, suggesting that photodegradation reactions followed the pseudo-first-order kinetics, $\ln(C_0/C) = k_{app}t$, where C_0 represents the initial concentration of MB and C denotes the concentration at a given reaction time 't'[7]. The apparent rate constant (k_{app}) and coefficient of determination (R^2) for the photocatalytic reactions of MB are given in Table 2.

To understand the role of active species responsible for the MB dye degradation over Cu-KTTO catalyst, a series of controlled experiments with different scavengers were investigated, and the results are

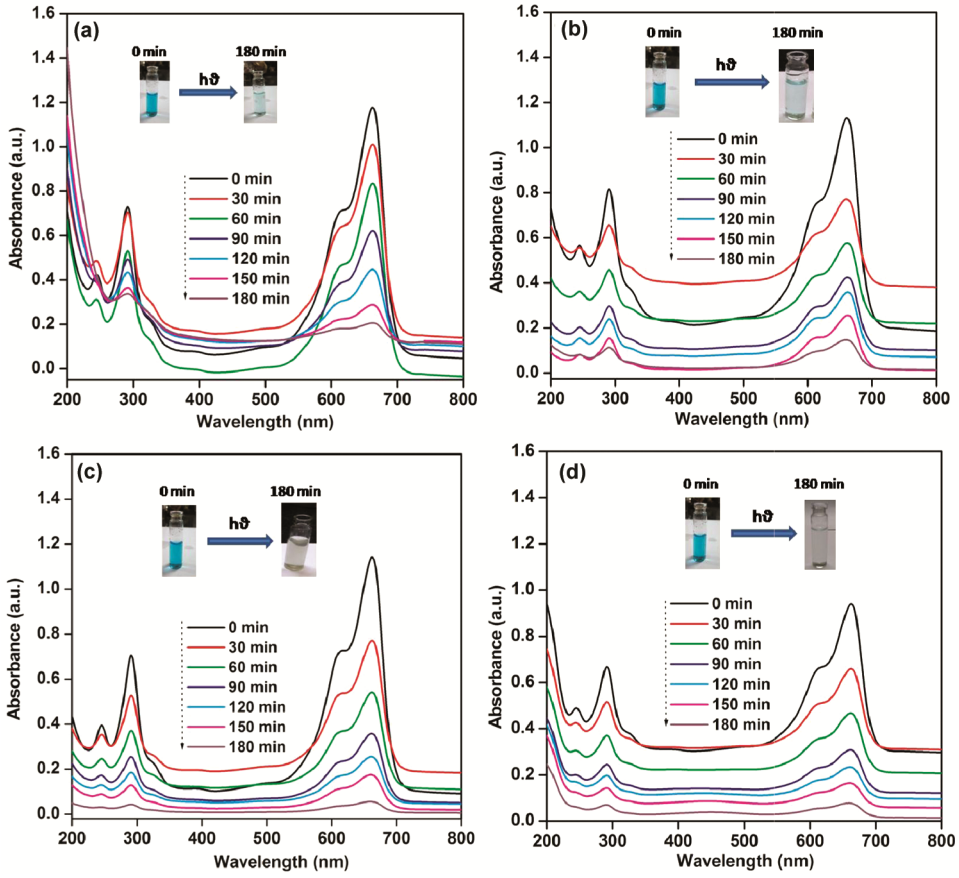

Fig. 7 — UV-visible absorption spectra of MB at different time intervals in the presence of (a) KTTO, (b) Ni-KTTO, (c) Cu KTTO and (d) Zn-KTTO (The inserted photographs illustrate the color change of MB solution during the reaction)

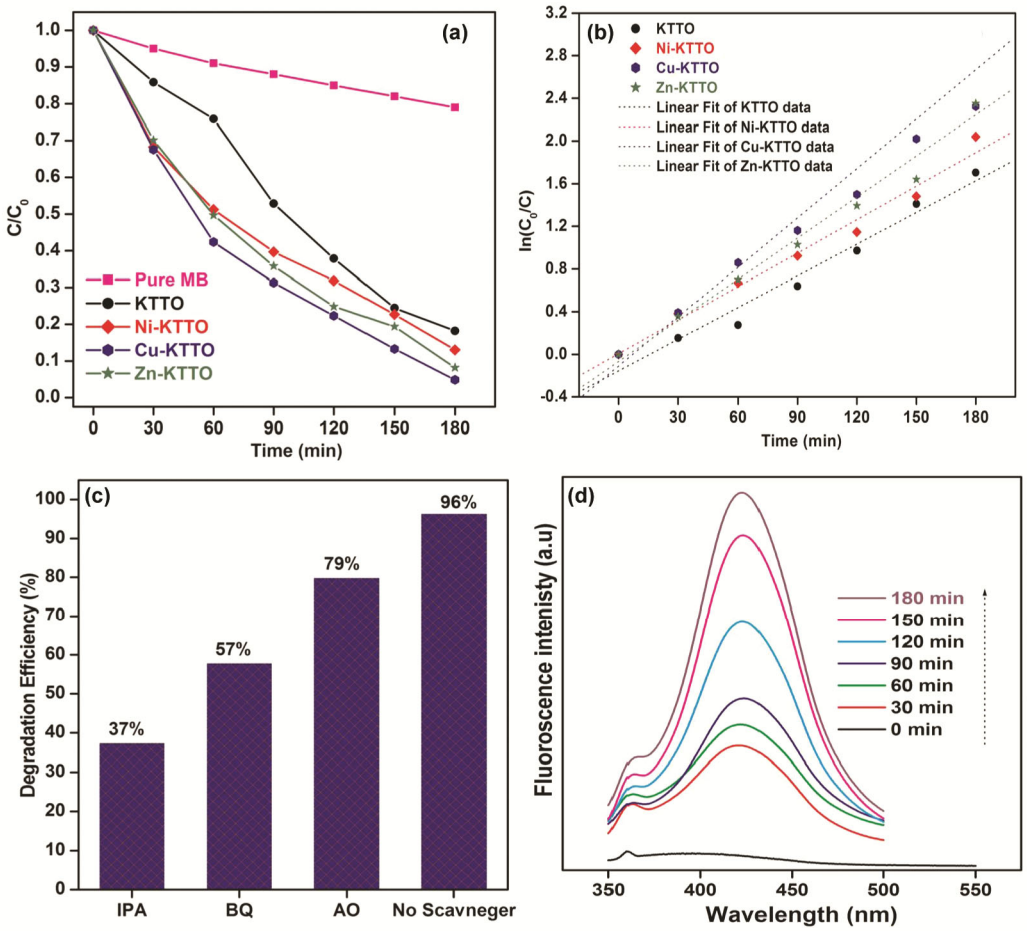

Fig. 8 — (a) Variation of concentration of MB with irradiation time, (b) the pseudo-first-order kinetics fitted curves of MB solution over KTTO, Ni-KTTO, Cu-KTTO and Zn-KTTO, (c) Effect of different scavengers on the degradation of MB in presence of the Cu-KTTO, and (d) Fluorescence spectra of visible light irradiated Cu-KTTO suspension in 3 mM terephthalic acid (λ_{exc} = 320 nm)

Table 2 — Kinetic parameters such as rate constant (k) and correlation coefficient (R^2) of KTTO, Ni-KTTO, Cu-KTTO and Zn-KTTO in the pseudo-first-order photocatalytic reaction

Sample	k (min^{-1})	(R^2)
KTTO	0.0099	0.9682
Ni-KTTO	0.0104	0.9820
Cu-KTTO	0.1543	0.9602
Zn-KTTO	0.1285	0.9689

shown in Fig. 8c. As shown in this figure, the degradation efficiencies of MB decreased from 96% to 37%, 57% and 79% in the presence of IPA (quencher of generated $^{\bullet}OH$), BQ (quencher of $^{\bullet}O_2^-$) and AO (quencher of and h^+), respectively, after 180 min of irradiation. The variation in the MB degradation from 96% to 37% in the presence of IPA suggests that $^{\bullet}OH$ radicals are major active species during the degradation of MB. In the presence of AO (scavenger for h^+), the MB degradation reduced to 79% (from 96%) and hence the role of h^+ in the decomposition of MB is minimum. Similarly, the contribution of superoxide radicals towards MB degradation is also less compared to that of $^{\bullet}OH$ radicals.

To further substantiate the formation of hydroxyl radicals on the surface of the Cu-KTTO catalyst, fluorescence experiments using terephthalic acid (TA) as a probe molecule, were carried out. It is documented that TA reacts with hydroxyl radicals and forms 2-hydroxy terephthalic acid (2-TAOH) which gives a characteristic emission signal at 425 nm in its fluorescence spectrum[23]. Fig. 8d shows the change in the fluorescence intensity as a function of visible light irradiation time for Cu-KTTO in 3 mM TA solution. A gradual increase in fluorescence intensity at 425 nm is observed with increasing irradiation time, which indicates an increase in the generation of $^{\bullet}OH$ on the catalyst surface during photocatalytic activity.

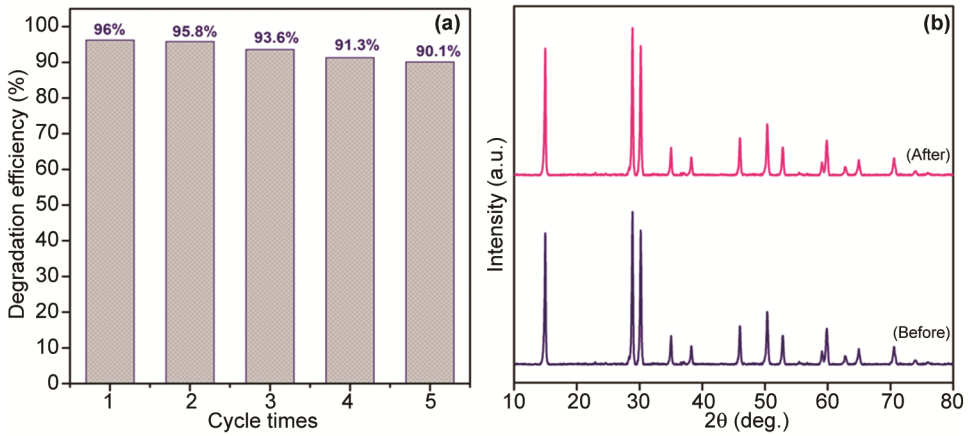

Fig. 9 — (a) Photocatalytic recycling experiments within five consecutive cycles using Cu-KTTO sample for the MB degradation and (b) Powder XRD patterns of the Cu-KTTO before and after the fifth cycle of photocatalytic experiment

Important properties for the viability of photocatalysts are chemical stability and the ability to re-use them[30]. In the present investigation, cyclic experiments were carried out to access the stability and reusability of the catalysts. After the first cycle, the used catalyst was separated, washed with distilled water and used in the second cycle with a fresh batch of MB solution. A similar procedure was followed for the third, fourth and fifth cycles. Fig. 9a shows the degradation of MB in the presence of Cu-KTTO catalyst for five successive cycles. As displayed in this figure, after five cycles, the Cu-KTTO sample still exhibits high photocatalytic performance and the photocatalytic degradation of MB is 90.1%, which indicates the Cu-KTTO has high chemical stability and can be reused at least up to five cycles. Furthermore, as shown in XRD results (Fig. 9b), the XRD pattern of the used catalyst after five cycles is similar to that of before photoreaction, further implying that the Cu-KTTO has good structural stability.

Based on the above characterization results, a plausible mechanism for MB degradation over Cu-KTTO under visible light irradiation is proposed and shown in Fig. 10. Upon absorption of visible light by the Cu-KTTO, the electrons in the valence band (VB) can be excited to the conduction band thereby leaving behind holes in the VB. The dopant Cu^{2+} can function as trapping centers for photogenerated electrons, which prevents the recombination with holes; thus, extending the lifetime of charge carriers[31]. The trapped electron is further scavenged by adsorbed oxygen to generate superoxide radical anions. These $^{\bullet}O^{2-}$ radicals can undergo protonation to form the $HO_2^{\bullet}$ and subsequently hydrogen peroxide and finally

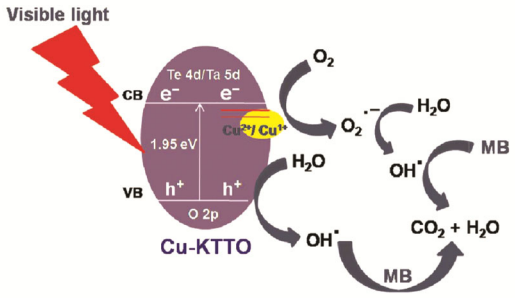

Fig. 10 — Schematic illustration for the photocatalytic degradation of MB using Cu-KTTO under visible light irradiation

results in the formation of $^{\bullet}OH$. The holes generated in the VB react with surface-bound water to produce the highly reactive hydroxyl radical. The $^{\bullet}OH$ radical is a powerful oxidizing agent that can attack MB molecules; as a result, MB was efficiently removed from wastewater. The following equations describe the mechanism of dye degradation.

$$KTTO \rightarrow KTTO_{VB}(h^+) + KTTO_{CB}(e^-) \quad \ldots (1)$$

$$Cu^{2+}(KTTO) + e^- \rightarrow Cu^{1+}(KTTO) \quad \ldots (2)$$

$$Cu^{+1}(KTTO) + O_2 \rightarrow Cu^{2+}(KTTO) + \dot{O}_2^- \quad \ldots (3)$$

$$e^- + O_2 \rightarrow \dot{O}_2^- \quad \ldots (4)$$

$$\dot{O}_2^- + H_2O + H^+ \rightarrow \dot{H}_2O_2 + O_2 \quad \ldots (5)$$

$$H_2O_2 + \dot{O}_2^- \rightarrow \dot{O}H + OH^- + O_2 \quad \ldots (6)$$

$$KTTO_{VB}(h^+) + H_2O \rightarrow \dot{O}H \quad \ldots (7)$$

$$\dot{O}H + MB molecules \rightarrow CO_2 + H_2O \quad \ldots (8)$$

Conclusions

In this work, the transition metal ions (Ni^{2+}, Cu^{2+}, and Zn^{2+}) doped $KTaTeO_6$ with defect pyrochlore structure have been successfully synthesized by a facile ion-exchange method. The XRD results confirmed the cubic structure of $KTaTeO_6$ which remains unchanged after doping of transition metal ions. The slight shift in the diffraction peaks towards higher Bragg's angle and red-shift in the absorption edges indicate the doping of transition metal ions into $KTaTeO_6$ lattice. The transition metal ions doping into KTTO lattice is confirmed from the presence of Ni, Cu, and Zn elemental peaks in their EDX profiles. The PL analysis confirmed the significant suppression of photogenerated charge carriers in doped KTTO samples. The impurity energy level formed by Cu^{2+} doping acts as electron trapping centers in the $KTaTeO_6$ lattice. This process reduces the recombination rate of photogenerated charge carriers and promotes their separation efficiency. The photocatalytic activities of resultant samples were evaluated by the degradation of MB under visible light irradiation. All the transition metal doped KTTO exhibited higher MB degradation efficiency than the parent KTTO under visible light and their photocatalytic activity follows the order of Cu-KTTO > Zn-KTTO > Ni-KTTO > KTTO. The relatively higher photocatalytic activity of Cu-KTTO can be attributed to its lower bandgap energy and effective reduction in the rate of electron-hole recombination. The results of trapping experiments and the TA probe method proved that the $^{\bullet}OH$ species played a key role in the degradation of MB over the Cu-KTTO. The highly active Cu-KTTO catalyst is stable and can be used cyclically up to five cycles for photodegradation of MB. These results open up new opportunities for various transition metal ions doped oxide photocatalytic systems particularly in the decomposition of environmental pollutants.

Supplementary Data

Supplementary data associated with this article are available in the electronic form at http://nopr.niscair.res.in/jinfo/ijca/IJCA_60A(06)812-823_SupplData.pdf.

Acknowledgment

MS gratefully acknowledges the funding agency, University Grant Commission (UGC), India, for providing financial support, in the form of SERO/UGC. The Science and Engineering Research Board (SERB) (Grant No. EMR/2016/001533), Department of Science and Technology (DST), India, is now acknowledged for its financial support. MV thanks CSIR, New Delhi for the award of Emeritus Scientist [21(1115)/20/EMR-II].

References

1 Venkataswamy P, Manasa S, Ravi G, Radha V & Vithal M, *Catal Lett,* 149 (2019) 2332.
2 Sreenu K, Venkataswamy P, Ravi G, Reddy C S, Reddy B J & Vithal M, *Z Anorg Allg Chem*, 645 (2019) 529.
3 Venkataswamy P, Jampaiah D, Kandjani A E, Sabri Y M, Reddy B M & Vithal M, *Res Chem Intermed*, 44 (2018) 2523.
4 Zhang W L, Li Y, Wang C & Wang P F, *Desalination*, 266 (2011) 40.
5 Sudheera M, Ravinder G, Ravi G, Venkataswamy P, Vaishnavi K, Chittibabu N & Vithal M, *Indian J Chem*, 59A (2020) 1092.
6 Manasa S, Ravi G, Venkataswamy P, Vaishnavi K & Vithal M, *SN Appl Sci*, 1 (2019) 1046.
7 Reddy J R, Ravi G, Kumar V N, Ravinder G & Vithal M, *J Chem Tech Biotech*, 90 (2015) 1937.
8 Smirnova O, Kumada N, Yonesaki N & Kinomura N, *Electrochem Commun*, 10 (2008) 485.
9 Moeller T, Clearfield A & Harjula R, *Chem Mater*, 13 (2001) 4767.
10 Moeller T, Clearfield A & Harjula R, *Micropor Mesopor Mater*, 54 (2002) 187.
11 Britvin S N, Siidra O I, Lotnyk A, Krivovichev S V & Depmeier W, *Eur J Inorg Chem*, 2010 (2010) 1082.
12 Ravinder G, Ravi G, Ramaswamy K, Sreenu K, Reddy C S, Malathi M, Radha V & Vithal M, *Indian J Chem*, 55A (2016) 1174.
13 Waehayee A, Watthaisong P, Wannapaiboon S, Chanlek N, Nakajima H, Wittayakun J, Suthirakun S & Siritanon T, *Catal Sci Technol*, 10 (2020) 978.
14 Venkataswamy P, Sudhakar Reddy Ch, Ravi G, Sadanandam G, Kumar V N & Vithal M, *Electron Mater Lett*, 14 (2018) 446.
15 Qi K, Xing X, Zada A, Li M, Wang Q, Liu S, Lin H & Wang G, *Ceram Int*, 46 (2020) 1494.
16 Devi L G, Nagaraju K, Narasimha B, Murthy & Kumar S G, *J Molec Catal A Chem*, 328 (2010) 44.
17 Yakout S M, *J Environ Chem Eng*, 8 (2020) 103644.
18 Venkataswamy P, Sudheera M, Vaishnavi K, Ramaswamy K, Ravi G & Vithal M, *J Electron Mater*, 49 (2020) 2358.
19 Dhiman M, Bhukal S, Chudasama B & Singhal S, *J Sol-Gel Sci Technol*, 81 (2017) 831.
20 Devi L G, Nagaraju K, Kumar S G & Rajashekhar K E, *Central Eur J Chem*, 8 (2010) 142.
21 Fukina D G, Suleimanov E V, Yavetskiy R P, Fukin G K, Boryakov A V, Borisov E N, Borisov E V, Surodin S I & Saharov N V, *J Solid State Chem*, 241 (2016) 64.
22 Bhat V & Gopalakrishnan J, *J Solid State Chem*, 63 (1986) 278.
23 Ravinder G, Ravi G, Reddy J R, Kumar V N, Sreenu K & Vithal M, *Photochem Photobiol*, 92 (2016) 223.

24 Maczka M, Knyazev A V, Kuznetsov N Y, Ptaka M & Macalik L, *J Raman Spectrosc*, 42 (2011) 529.

25 Atuchin V, Kesler V, Meng G & Lin Z, *J Phys Condens Matter*, 24 (2012) 405503.

26 Shi R, Lin J, Wang Y, Xu J & Zhu Y, *J Phys Chem C*, 114 (2010) 6472.

27 Chaudhary P & Ingole P P, *Electrochim Acta*, 357 (2020) 136798.

28 Zheng M, Xing C, Zhang W, Cheng Z, Liu X & Zhang S, *Inorg Chem Commun*, 119 (2020) 108040.

29 Li H, Zhou Y, Tu W, Ye J & Zou Z, *Adv Funct Mater*, 25 (2015) 998.

30 Kumar V N, Reddy J R, Ravi G, Ravinder G, Radha V, Venkataswamy P & Vithal M, *ChemistySelect*, 1 (2016) 2783.

31 Qi K, Xing X, Zada A, Li M, Wang Q, Liu S, Lin H & Wang G, *Ceram Int*, 46 (2020) 1494.